RESEARCH ARTICLE | AUGUST 09 2024

Decoherence ensures convergence of non-adiabatic molecular dynamics with number of states *⊗*

Special Collection: Algorithms and Software for Open Quantum System Dynamics

Dongyu Liu ⁽ⁱ⁾; Bipeng Wang ⁽ⁱ⁾; Andrey S. Vasenko ⁽ⁱ⁾; Oleg V. Prezhdo ⁽ⁱ⁾



J. Chem. Phys. 161, 064104 (2024) https://doi.org/10.1063/5.0222557

A CHORUS





Articles You May Be Interested In

Mixed quantum-classical equilibrium in global flux surface hopping

J. Chem. Phys. (June 2015)

Communication: Global flux surface hopping in Liouville space

J. Chem. Phys. (November 2015)

Branching and phase corrected surface hopping: A benchmark of nonadiabatic dynamics in multilevel systems

J. Chem. Phys. (June 2021)





Decoherence ensures convergence of non-adiabatic molecular dynamics with number of states

Cite as: J. Chem. Phys. 161, 064104 (2024); doi: 10.1063/5.0222557 Submitted: 8 June 2024 • Accepted: 24 July 2024 • **Published Online: 9 August 2024**













Dongyu Liu, Dongyu Liu, Dang Wang, Dandrey S. Vasenko, Dand Oleg V. Prezhdo Dandrey S. Vasenko, Dandrey S.





AFFILIATIONS

- 1 HSE University, 101000 Moscow, Russia
- ²Department of Chemical Engineering, University of Southern California, Los Angeles, California 90089, USA
- ³Donostia International Physics Center (DIPC), 20018 San Sebastián-Donostia, Euskadi, Spain
- ⁴Department of Chemistry, University of Southern California, Los Angeles, California 90089, USA
- Department of Physics and Astronomy, University of Southern California, Los Angeles, California 90089, USA

Note: This paper is part of the JCP Special Topic on Algorithms and Software for Open Quantum System Dynamics.

a) Authors to whom correspondence should be addressed: avasenko@hse.ru and prezhdo@usc.edu

ABSTRACT

Non-adiabatic (NA) molecular dynamics (MD) is a powerful approach for studying far-from-equilibrium quantum dynamics in photophysical and photochemical systems. Most NA-MD methods are developed and tested with few-state models, and their validity with complex systems involving many states is not well studied. By modeling intraband equilibration and interband recombination of charge carriers in MoS₂, we investigate the convergence of three popular NA-MD algorithms, fewest switches surface hopping (FSSH), global flux surface hopping (GFSH), and decoherence induced surface hopping (DISH) with the number of states. Only the standard DISH algorithm converges with the number of states and produces Boltzmann equilibrium. Unitary propagation of the wave function in FSSH and GFSH violates the Boltzmann distribution, leads to internal inconsistency between time-dependent Schrödinger equation state populations and trajectory counts, and produces non-convergent results. Introducing decoherence in FSSH and GFSH by collapsing the wave function fixes these problems. The simplified version of DISH that omits projecting out the occupied state and is applicable to few-state systems also causes problems when the number of states is increased. We discuss the algorithmic application of wave function collapse and Boltzmann detailed balance and provide detailed FSSH, GFSH, and DISH flow charts. The use of convergent NA-MD methods is highly important for modeling complicated quantum processes involving multiple states. Our findings provide the basis for investigating quantum dynamics in realistic complex systems.

Published under an exclusive license by AIP Publishing. https://doi.org/10.1063/5.0222557

INTRODUCTION

Non-adiabatic (NA) molecular dynamics (MD) enables realtime modeling of far-from-equilibrium quantum dynamics processes in various systems, representing a promising approach for investigating key charge and energy transfer processes in many important photophysical and photochemical systems. In this approach, essentially quantum particles, such as electrons and protons, are described fully quantum mechanically, while the remaining parts are treated with classical mechanics or semi-classically to reduce the computational cost, leading to the so-called mixed quantum-classical dynamics.⁸⁻¹¹ Due to its desirable computational accuracy and efficiency, NA-MD has been widely employed in a

number of applications, such as photoinduced chemical reactions and photogenerated carrier relaxation and recombination. 12-15 NA-MD mimics most directly nature and time-resolved experiments, by providing an atomistic description of the processes explicitly in the time domain. The computational cost of NA-MD is typically limited by quantum-mechanical calculations, and the systems are usually simplified to small models and few quantum states, resulting in a gap between experimental and theoretical research. In recent years, with the development of advanced theoretical and computational methods, especially machine learning, 16,17 simulating large and complex systems at the quantum-mechanical level is becoming feasible,¹ paving the way for using NA-MD to investigate quantum dynamics under more realistic conditions. In these systems, a large number of states are expected to participate in the quantum processes because the density of states is proportional to the number of atoms. However, most NA-MD methods are derived and tested with few-state models, and the impacts of including multiple states are rarely considered. To conjugate NA-MD with state-of-the-art computational techniques for simulating the quantum dynamics in large and complex systems, it is essential to revisit the computational validity of NA-MD approaches, including convergence with the number of states.

Excited state dynamics in condensed phase and nanoscale systems involve many degrees of freedom, allowing for efficient energy exchange and dissipation. Over time, the systems approach Boltzmann equilibrium, and quantum transitions occur primarily to the states with similar or lower energies. Higher energy states can only be accessed transiently, and therefore, one can expect convergence of NA-MD simulations with the number of states. Including many states into NA-MD simulations is essential for modeling nanoscale and condensed phase systems, because high densities of states, in combination with the enhancement of electron-electron and electron-phonon coupling by quantum confinement, give rise to novel and important phenomena.7 For instance, quantum dots exhibit remarkable and tunable properties, compared with bulk and molecular systems, because of the quantum confinement effect.²⁵ Simulations demonstrate such confinement changes not only gaps but also couplings between states, synergistically regulating exciton relaxation and recombination dynamics. 26,27 Valleytronics is an emerging information processing and storage technology that works by manipulating the occupancy of energy valleys in the band structure. 28 Different valleys are separated in the continuous momentum space, and a sufficient number of states need to be considered for modeling intervalley transitions.²⁹ Excitons in semiconductor Moiré superlattices have attracted tremendous attention in recent years for advanced optoelectronics applications. 30 These excitons are strongly coupled across the heterojunction of 2D materials and exhibit resonant tunneling, involving many states near the band edge from each component.³¹ In these systems, the evolution from non-equilibrium to equilibrium is intermediated by many quantum states, requiring enough states in NA-MD simulations to cover all possible transition channels. Therefore, to model such complex quantum processes using NA-MD and to elucidate the relevant mechanisms, the convergence with the number of states needs to be studied in

In this work, we investigate the convergence of several NA-MD methods with respect to the number of states used in the simulations, taking the intraband carrier equilibration and interband recombination in monolayer MoS₂ as an example. MoS₂ is a representative 2D semiconductor with many promising electronic and optoelectronic applications. 32-34 Upon electron excitation from the valence band (VB) to the conduction band (CB), the carriers, i.e., the electron and hole, relax rapidly to the CB minimum (CBM) and the VB maximum (VBM) and then go through a relatively slow interband recombination. Due to thermal excitation, carriers populate multiple states near the CBM and VBM, generating additional recombination channels and affecting the dynamics. We test fewest switches surface hopping (FSSH),³⁵ global flux surface hopping (GFSH),³⁶ and decoherence-induced surface hopping (DISH),³⁷ which have been widely employed to study excited-state dynamics in molecular and condensed matter systems.^{38–40} We find that FSSH and GFSH do not converge, because overcoherence leads to unphysical wave function propagation to higher energy states, and that collapsing the wave function can fix this problem. DISH intrinsically avoids this issue by considering decoherence in the wave function propagation, but the decoherence events need to be correctly incorporated with the energy conservation requirement. We demonstrate that a commonly used DISH simplification violates the Boltzmann distribution in the presence of multiple states close in energy and produces non-convergent results. The original DISH works fine, converging and producing the Boltzmann equilibrium. We also show that including more states near band edges can notably influence carrier recombination by providing additional decay channels. The findings generate critical insights into understanding the convergence in NA-MD simulations and serve as a cornerstone for investigating quantum dynamics in large-scale and complex systems.

METHODS

NA-MD simulations require evolution of the wave function of quantum particles and a trajectory of the classical particles. The quantum (e.g., electrons) and classical (e.g., vibrations) subsystems are coupled. The classical subsystem creates an external that enters the quantum Hamiltonian and generates inelastic (quantum transitions) and elastic (decoherence) events. The quantum subsystem creates a force on the classical subsystem that evolves on a potential energy surface (PES). The force can be average, as in the Ehrenfest/mean-field approach, or state-specific, as in surface hopping (SH). Alternatively, the trajectory can be pre-computed, as in the classical path approximation (CPA), so invoking the neglect of back-reaction approximation (NBRA).

Evolution of quantum particles

The propagation of the wave function $\psi(\mathbf{r}, \mathbf{R}, t)$ follows the time-dependent Schrödinger equation (TD-SE),

$$i\hbar \frac{\partial \psi(\mathbf{r}, \mathbf{R}, t)}{\partial t} = H(\mathbf{r}; \mathbf{R})\psi(\mathbf{r}, \mathbf{R}, t),$$
 (1)

where \mathbf{r} and \mathbf{R} are the coordinates of quantum and classical particles, respectively. $H(\mathbf{r}; \mathbf{R})$ is the Hamiltonian of quantum particles and depends on the classical positions parametrically. The classical particles evolve according to a trajectory $\mathbf{R} = \mathbf{R}(t)$, making the Hamiltonian time-dependent operator $H(\mathbf{r}; \mathbf{R}(t))$. Using a set of orthonormal basis functions $\phi_i(\mathbf{r}; \mathbf{R})$, we define the matrix elements of $H(\mathbf{r}; \mathbf{R})$ as

$$V_{ij}(\mathbf{R}) = \langle \phi_i(\mathbf{r}; \mathbf{R}) | H(\mathbf{r}; \mathbf{R}) | \phi_j(\mathbf{r}; \mathbf{R}) \rangle$$
 (2)

and expand the wave function of quantum particles as

$$\psi(\mathbf{r}, \mathbf{R}, t) = \sum_{j} c_{j}(t)\phi_{j}(\mathbf{r}; \mathbf{R}), \qquad (3)$$

where $c_j(t)$ are the expansion coefficients. Substituting Eq. (3) into the TD-SE, Eq. (1), and multiplying by $\phi_k(\mathbf{r}; \mathbf{R})$ from the left give evolution of the coefficients,

$$i\hbar\dot{c}_k = \sum_j c_j (V_{kj} - i\hbar\dot{\mathbf{R}} \cdot \mathbf{d}_{kj}),$$
 (4)

where $\dot{\mathbf{R}} \cdot \mathbf{d}_{ki}$ is the non-adiabatic coupling (NAC),

$$\dot{\mathbf{R}} \cdot \mathbf{d}_{kj} = \left\langle \phi_k | \frac{\partial}{\partial t} | \phi_j \right\rangle = \left\langle \phi_k | \frac{\partial}{\partial \mathbf{R}} \frac{\partial \mathbf{R}}{\partial t} | \phi_j \right\rangle = \dot{\mathbf{R}} \langle \phi_k | \nabla_R | \phi_j \rangle. \tag{5}$$

The population change of each state can be expressed in density matrix notation as

$$\dot{a}_{kk} = \dot{c}_k c_k^* + c_k \dot{c}_k^* = \sum_{l,k} b_{kl}, \tag{6}$$

where

$$b_{kl} = 2\hbar^{-1}\operatorname{Im}(a_{kl}^*V_{kl}) - 2\operatorname{Re}(a_{kl}^*\dot{\mathbf{R}} \cdot \mathbf{d}_{kj}). \tag{7}$$

In this work, valence electrons are treated quantum-mechanically, and their wave functions are obtained by calculating the Kohn–Sham (KS) orbitals of density functional theory (DFT). Equation (1) is the TD-KS equation. The wave function is expanded in the basis of adiabatic KS orbitals, Eq. (3). The matrix elements V_{kj} of Eq. (7) vanish in this adiabatic representation.

FSSH, GFSH, and DISH

In SH approaches, quantum dynamics is modeled by hopping the system between different PESs and accumulating statistics from sufficient realizations. A detailed description of the SH algorithms is provided at the end of this article. The hopping probabilities are derived from the propagation of wave functions using the TD-SE. The SH probability expressions are derived to maintain consistency between SH populations of PESs and TD-SE population of states (squares of wave function expansion coefficients). FSSH and GFSH compute the hopping probabilities based on the quantum mechanical flux. After a sufficiently short time interval Δt , the flux of population from the currently occupied state i to another state j, normalized by the population of state i, can be calculated as $\Delta a_{i \rightarrow j}/a_{ii} = b_{ij}\Delta t/a_{ii}$. FSSH defines the hopping probabilities using this expression and sets the reverse flux to zero, which can be written as

$$g_{ij}^{\text{FSSH}} = \max\left\{\frac{-b_{ij}\Delta t}{a_{ii}}, 0\right\}.$$
 (8)

Because the FSSH probabilities explicitly depend on couplings between states that enter Eq. (7) for b_{ij} , this method does not allow transitions between indirectly coupled states, such as in the superexchange mechanism. GFSH captures these transitions^{36,43} by calculating the flux from the state populations directly. Specifically, GFSH divides the states into two subgroups based on their population changes over a sufficiently short time interval, $\Delta a_{ii} = a_{ii}(t + \Delta t) - a_{ii}(t)$, and the system is only allowed to hop from states with decreased populations (group A) to states with increased populations (group B). If the currently occupied state i belongs to group A, the hopping probability to another state j in group B is defined as

$$g_{ij}^{\text{GFSH}} = \frac{\Delta a_{jj}}{a_{ii}} \frac{\Delta a_{ii}}{\sum_{k \in A} \Delta a_{kk}} (\text{if } i \in A \text{ and } j \in B).$$
 (9)

The hopping within the same group or from group B to A is forbidden, and the relevant $g_{ij}^{\rm GFSH}$ is set to zero. After obtaining the

hopping probabilities from FSSH or GFSH at a given time step, a uniform random number $\xi \in (0,1)$ is used to decide which PES to switch to. If ξ satisfies $\sum_{j=1}^{j=k-1} g_{ij} < \xi < \sum_{j=1}^{j=k} g_{ij}$, the system is expected to switch to the PES of state k, otherwise the hopping is rejected.

The original FSSH and GFSH methods use the unitary TD-SE, leading to the overcoherence problem.⁴⁴ A simple solution is provided by collapsing the wave function to the newly occupied state after each hop.⁴⁵ Such an algorithm implies that the timescales of inelastic scattering (hop) and elastic scattering time (decoherence) are the same.

Rooted in the quantum dynamics of open systems, $^{46-49}$ DISH uses decoherence as the physical source of evolution branching. The hopping probabilities are calculated based on the squares of the wave function coefficients, rather than expressions, such as Eqs. (8) and (9), and hops can happen at decoherence events. The addition to the TD-SE, the wave function propagation in DISH is also determined by decoherence events, as in quantum dynamics of open systems. The decoherence time $\tau_i(t)$ of each state i is calculated as

$$\frac{1}{\tau_i(t)} = \sum_{j \neq i}^{N} |c_j(t)|^2 r_{ij}, \tag{10}$$

where r_{ij} is the rate of decoherence between states i and j, typically estimated as the pure-dephasing rate. ^{50,51} When the decoherence time of state i is reached, either the wave function collapses onto this state with the probability of $|c_i(t)|^2$, or state i is projected by setting $c_i(t)$ to zero and renormalizing the wave function. If the wave function collapses to a new state, the system switches the PES to this state. If the currently occupied state is projected out, the system switches to another PES based on the quantum probabilities $|c_i(t)|^2$. Hence, the DISH probabilities can be expressed as

$$g_{ij}^{\text{DISH}} = |c_j(t)|^2$$
 when $\tilde{t}_j \ge \tau_j$, or state j is projected out, (11)

where \tilde{t}_j is the time interval since the last decoherence event of state j.

It is important to note that elastic and inelastic electron-phonon scattering times are treated independently in DISH, as demonstrated by the following example. The decoherence rates are often estimated as pure-dephasing times using the optical response theory, on the basis of fluctuations of electronic energy levels, while DISH hopping probabilities are governed largely by NAC magnitudes. If initial and final states are localized on different parts of a system, the fluctuation of the energy gap between them can be rapid, resulting in fast coherence loss. However, the NAC is zero, because the corresponding wave functions are localized away from each other, and quantum transitions never happen.

Details of NA-MD and DFT calculations

NA-MD simulations were carried out using the Hefei-NAMD code within the real-time TD-KS framework.⁴⁰ The TD-SE was implemented in the KS representation as introduced above, and the quantum dynamics is modeled with FSSH, GFSH, and DISH. The CPA was adopted in NA-MD by assuming that the electronic excitation has little influence on the atomic motion of MoS₂, compared to thermal fluctuations.³⁸ This assumption is valid for many nanoscale

and condensed matter systems, indicating that the electronic structure evolution can be derived from ground state trajectories. Under the CPA, the energy conservation is realized by scaling the hopping probabilities with the Boltzmann factor instead of rescaling the velocities, and the needed scalar NACs can be easily calculated from the overlap of adiabatic wave functions. 38

The ground state trajectory of MoS2 was produced by performing ab initio MD (AI-MD) simulations with the Vienna initio Simulation Package (VASP). pro $method^{56-59} \\$ augmented-wave (PAW) and the Perdew-Burke-Ernzerhof (PBE) functional⁶⁰ were used describe the electron-ion interactions. The cutoff energy of the plane wave basis was set to 400 eV. The monolayer MoS₂ was represented by a 6×6 supercell with a vacuum layer of 15 Å, and only the Γ point was used to sample the Brillouin zone in AI-MD simulations. A 5 ps microcanonical trajectory with a time step of 1 fs was generated after heating the system to 300 K. The KS orbitals of the structures from this trajectory were then calculated using the OpenMX code. 61,62 The PBE functional and norm-conserving pseudopotentials were used for solving the KS equation.⁶³ The s3p2d1 and s2p2d1 pseudo-atomic orbital basis functions were assigned to Mo and S atoms, respectively. The tight-binding Hamiltonian was calculated with a $3 \times 3 \times 1$ k-point mesh, and the wave functions at the Γ point were used to calculate the NACs.⁶⁴ We employed both original and 10-times enlarged NACs to reduce the NA-MD simulation time, which accelerated the dynamics by about 100 times, according to our testing (see Fig. S1). We uniformly sampled 100 initial configurations from the AI-MD trajectory and employed 1000 SH realizations for each of them. The reported results were obtained by averaging the NA-MD results from all the 100 000 realizations. The populations of ground states, e.g., shown in Figs. 2(a), 2(b), 2(d), and 2(e), were calculated as the fraction of the realizations of the SH algorithm in that state. We also report TD-SE state populations, e.g., shown in Figs. 2(c) and 2(f), which are calculated by averaging the squares of the coefficients of the wave function over all realizations. These two sets of populations are not consistent in FSSH and GFSH without decoherence, while they are consistent in FSSH and GFSH with decoherence and in DISH.

RESULTS AND DISCUSSION

Electronic structure of monolayer MoS₂

Figure 1(a) displays the geometric structure of monolayer MoS_2 with different simulation cell sizes as indicated by the blue frames, and Fig. 1(b) shows the corresponding band structure near the CBM and VBM. Monolayer MoS_2 is a direct bandgap semiconductor with both CBM and VBM at the K point of the Brillouin zone of the primitive cell. For AI-MD simulations, the small primitive cell leads to severe finite-size effects such as exaggerating thermal fluctuations and reflecting only a few Γ point phonons. Moreover, the NACs between non- Γ point wave functions cannot be calculated directly because of the phase factor in the Bloch function.²⁹ Tripling the unit cell folds the VBM and CBM to the Γ point, which alleviates the phase factor issue and finite-size effects. Meanwhile, more states appear at the band edge, and both VBM and CBM become degenerate. Further enlarging the simulation cell can improve the accuracy

of NA-MD simulations by including more vibrational motions and electronic states, but the DFT calculations become costly. Hence, a 6 \times 6 supercell is adopted to balance the computational accuracy and cost. Compared with the band structure of the 3 \times 3 model, several states are introduced above the CBM and below the VBM, reducing the intraband energy gaps and modifying the electronic structure significantly. Figure 1(c) displays the evolution of the Γ point energy levels over 1 ps under thermal fluctuations. CBM and CBM + 1 remain degenerate, while VBM and VBM - 1 separate in energy. In addition, the energy gaps within the CB almost disappear, well representing a continuous energy band. The 5 ps energy level evolution results are shown in Fig. S2.

FSSH and GFSH simulations

FSSH and GFSH are studied together because the hopping probabilities of both algorithms are derived from the wave function flux. We test their convergence by modeling electron–hole recombination dynamics in MoS₂ with an increasing number of CB or VB states. Specifically, we set the CBM (VBM) as the initial state of the electron (hole) and include more states above (below) in energy in the NA-MD simulations. We consider the states up to CBM + 20 and down to VBM - 20. The corresponding energy levels can be found in Fig. S2(a). The energy ranges of the considered states are much larger than $k_{\rm B}T$ at 300 K (about 0.026 eV), indicating that the high energy states should not be occupied according to the Boltzmann distribution. Therefore, the NA-MD simulation results should converge after including a sufficient number of states.

Figures 2(a) and 2(b) display the charge recombination dynamics from the FSSH and GFSH simulations, respectively, in the basis including the VBM and a varying number of CB states. Neither method converges with an increasing number of states. The recombination becomes faster in FSSH when more CB states are included, and the GFSH recombination shows a non-monotonic dependence on the number of states. The evolutions of the wave function populations, i.e., $c_i(t)$ squares, obtained from the TD-SE, Eqs. (1) and (4), and the expectation value of the electron energy with CB states up to CBM + 20 are plotted in Fig. 2(c). The TD-SE evolution results are identical in FSSH and GFSH, and the longer 5 ps data can be found in Fig. S3. The electron wave function evolves from the CBM to higher energy states within several picoseconds, increasing the energy expectation value by about 0.3 eV. The energy growth by over 10 k_BT violates the Boltzmann distribution, and the wave function unphysically "leaks" from the CBM to higher energy states. Changes in the populations of the CB states influence electron hop to the VBM, leading to charge recombination, even though the NACs from all CB states to the VBM are comparable; see Fig. S2(b). Moreover, the average root-mean-square (rms) value of the NACs between adjacent CB states is 0.076 eV, which is larger than k_BT at 300 K, indicating that the system is not in the weak coupling limit for the intraband processes. Therefore, the concept of Boltzmann equilibrium within the finite size representation of the bands is applicable only approximately, because energy gaps are not much larger than couplings between states. Similarly, the rms NAC between adjacent VB states is 0.068 eV, also larger than k_BT at 300 K. In FSSH, the hopping probabilities depend on both the NACs and the ratio between the density matrix elements a_{ij}^*/a_{ij} , Eq. (8). If the population of the occupied state, e.g., the CBM, a_{ii} is reduced, the

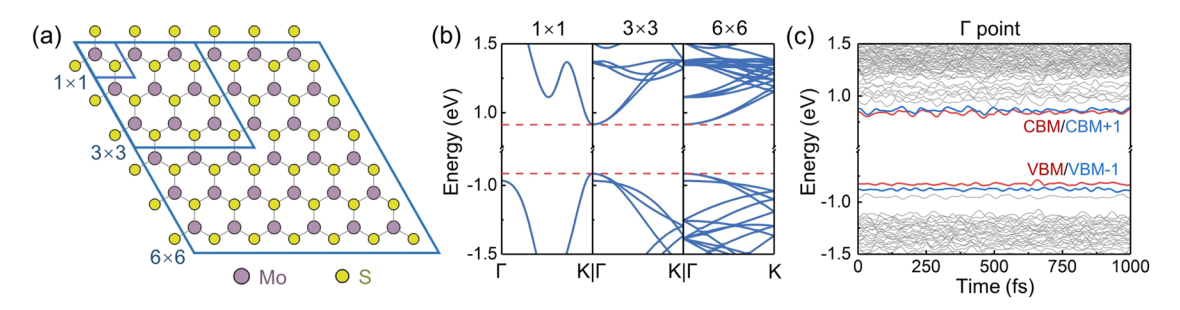


FIG. 1. (a) Geometric and (b) band structure of monolayer MoS_2 for different simulation cell sizes. The VBM and CBM positions are indicated by red dashed lines. (c) Evolution of the Γ point energy levels of the 6 \times 6 MoS_2 model at 300 K. The bandgap center is set to 0 eV. The intraband energy gaps almost disappear in the CB but are maintained in the VB under thermal fluctuations.

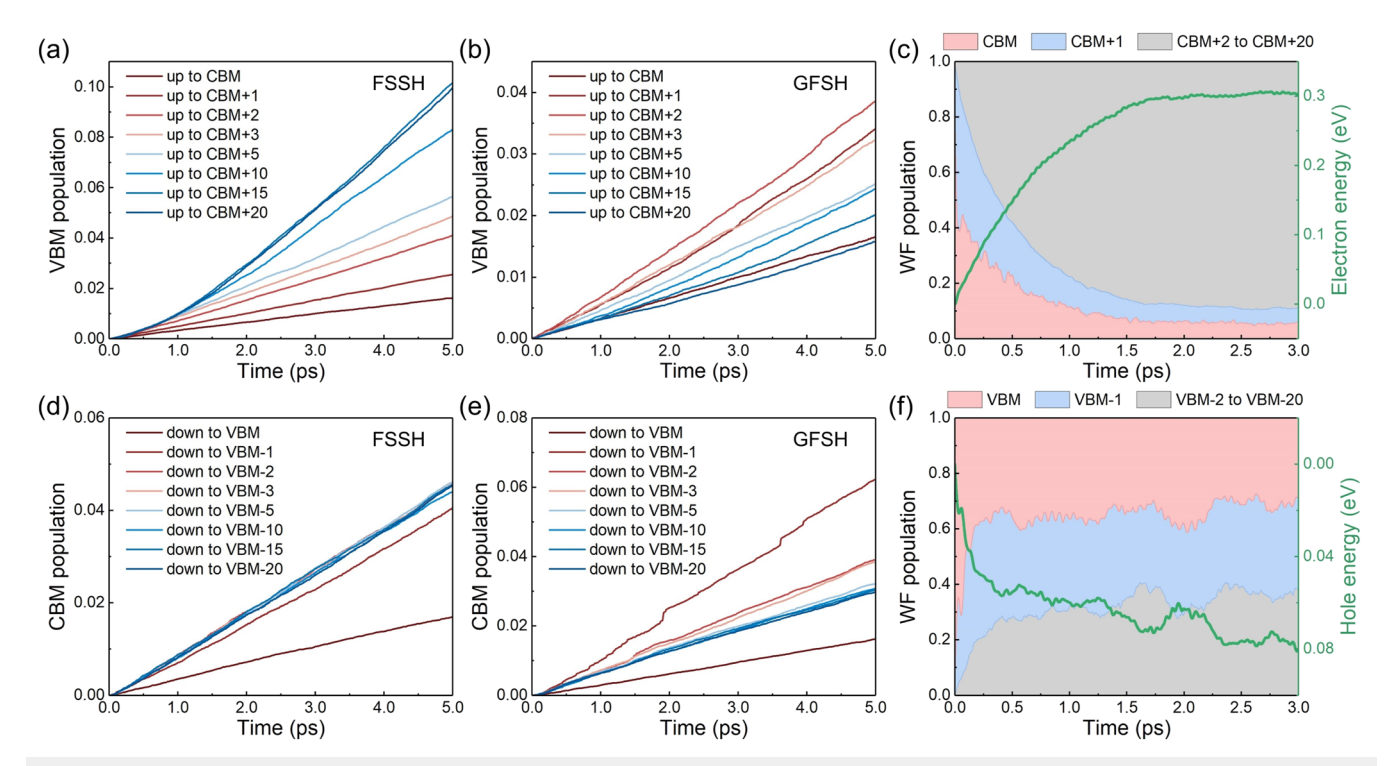


FIG. 2. Results for original FSSH and GFSH without decoherence. (a) FSSH and (b) GFSH simulations of electron–hole recombination dynamics in the basis including VBM and different numbers of CB states. (c) Evolutions of TD-SE state populations and the expectation value of the electron energy with the CB states up to CBM + 20. Longer time data are shown in Fig. S3. The CBM energy is set to 0. Charge recombination dynamics does not converge with the number of CB states, panels (a) and (b). The populations spread artificially to high energy states, and the average electron energy grows artificially high, more than 10 k_BT above the CBM. At room temperature, k_BT = 0.026 eV. (d) FSSH and (e) GFSH simulations of electron–hole recombination dynamics in the basis including CBM and different numbers of VB states. (f) Evolutions of TD-SE state populations and the energy expectation value of the hole with the VB states down to VBM - 20. The VBM energy is set to 0. There is convergence with the number of VB states, panels (d) and (e). However, the hole energy grows multiple k_BT away from the VBM instead of decaying toward it, panel (f), indicating that the convergence is unphysical, violating the Boltzmann distribution.

hopping probability to VBM is enlarged, and the recombination is therefore accelerated. The relationship between the TD-SE state populations and the GFSH hopping probabilities is more complicated. On the one hand, the reduced a_{ii} increases the $\Delta a_{ij}/a_{ii}$ term in Eq. (9). On the other hand, the reduced a_{ii} decreases the contribution flux from state i to the global flux, i.e., the $\Delta a_{ii}/\sum_{k \in A} \Delta a_{kk}$ term

in Eq. (9). Because the GFSH hopping probabilities are calculated as the product of these two terms, the final recombination rates depend on the competition between them, leading to a non-monotonic dependence.

The dependence of the electron-hole recombination dynamics on the number of VB states is shown in Figs. 2(d) and 2(e). Both

FSSH and GFSH results converge. Figure 2(f) displays the evolutions of the wave function populations and the expectation value of the hole energy with VB states down to VBM -20. The wave function remains mostly in VBM and VBM -1, because of the large energy gap from VBM -1 to VBM -2, Fig. 1(c). However, the hole energy increases by much more than $k_{\rm B}T$ at 300 K, violating the Boltzmann distribution. Therefore, the convergence of the hole recombination dynamics in the FSSH and GFSH simulations is unphysical. Indeed, realistic semiconductors have continuous VB and CB, indicating that the wave function leaking issue observed with an increasing number of CB states is a general case.

The lack of convergence can be attributed to the lack of decoherence in FSSH and GFSH and the unitary nature of the TD-SE. The TD-SE does not satisfy the detailed balance between transitions upward and downward in energy and is independent of the Boltzmann factor. The wave function can propagate freely to any state regardless of energy differences. In particular, the small energy gaps between the adjacent CB states in MoS₂ result in large NACs and lead to fast spreading of the wave function overall all CB states present in the simulation. However, hopping to higher energy PESs is suppressed by the Boltzmann factor, causing a discrepancy

between the SH and TD-SE state populations. Decoherence can fix this issue by modifying the wave function amplitudes during the propagation. The overcoherence problem was extensively investigated before, and various methods have been proposed to introduce decoherence effects. 44 Here, we project the wave function onto the newly occupied state once a hopping is accepted, known as instantaneous decoherence after successful hops (ID-S). 45 This approach synchronizes the TD-SE and SH populations constantly, thus preventing the wave function from leaking to higher energy states. The FSSH and GFSH simulation results with the wave function collapse are plotted in Fig. 3. The recombination dynamics of both electrons and holes converge with the number of states, and the trends are consistent with the above discussion. Figures 3(c) and 3(f) show that the electron and hole energies reach maxima after about 0.2 ps, with the energies relative to the band edges comparable to $k_{\rm B}T$ at 300 K, representing thermal excitation. The wave function populations are dominated by the low energy states, demonstrating that the wave function leaking issue is fixed, as shown in Figs. 3(c) and 3(f) for FSSH and Fig. S4 for GFSH. The longer simulation data can be found in Figs. S5 and S6.

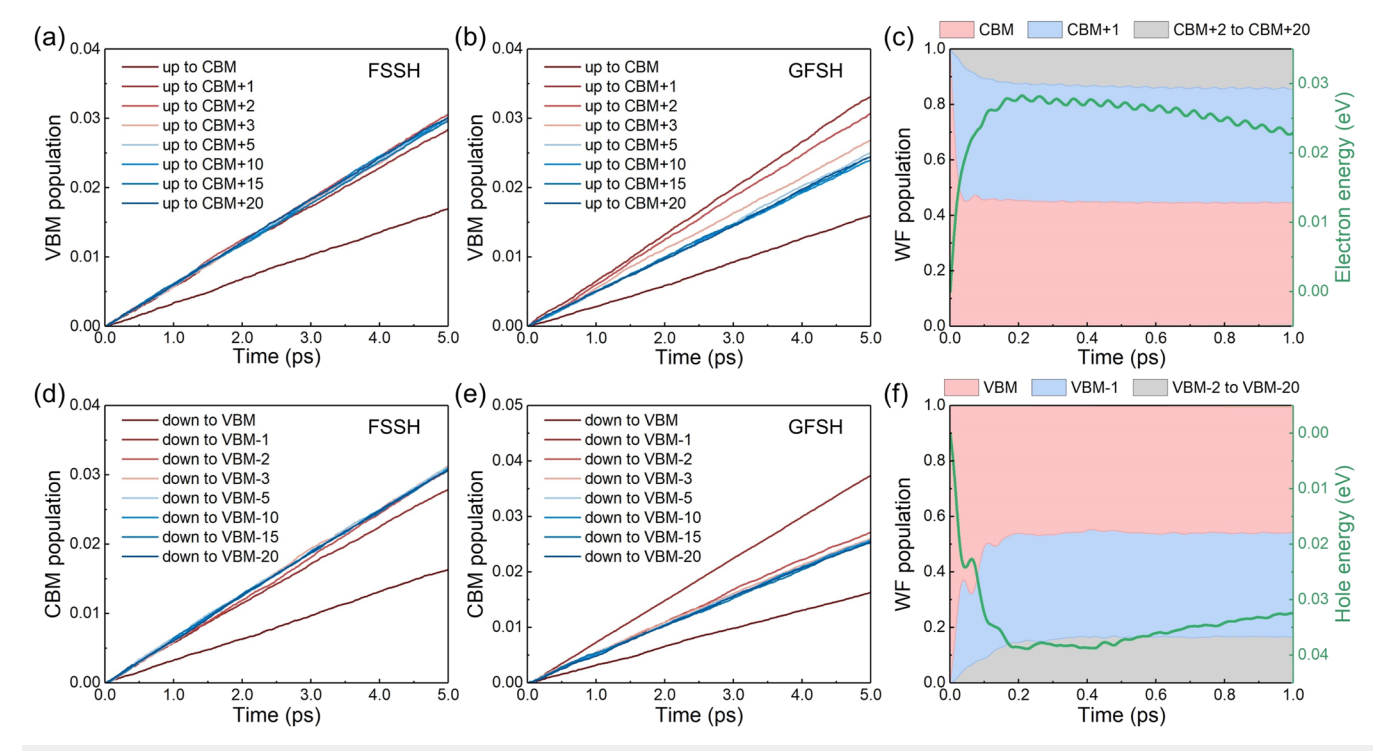


FIG. 3. Results for FSSH and GFSH with decoherence. The wave function collapses to the occupied state after each hop. (a) FSSH and (b) GFSH simulations of electron–hole recombination dynamics in the basis including VBM and different numbers of CB states. (c) FSSH evolutions of TD-SE state populations and the expectation value of the electron energy with the CB states up to CBM + 20. Corresponding GFSH results are shown in Fig. S4. The charge recombination dynamics converges with the number of CB states, panels (a) and (b). The populations are dominated by low energy states, and the electron energy is with k_BT and decays toward the CBM, panel (c), as should be expected. (d) FSSH and (e) GFSH simulations of electron–hole recombination dynamics in the basis including CBM and different numbers of VB states. (f) FSSH evolutions of TD-SE state populations and the energy expectation value of the hole with the VB states down to VBM - 20. The charge recombination dynamics converges with the number of VB states, panels (d) and (e). The populations are dominated by low energy states, and the hole energy decays toward the VBM, panel (f), as should be expected. Longer FSSH/GFSH data with decoherence are shown in Figs. S5 and S6.

DISH simulations

When we collapse the wave function after a hop is accepted in FSSH and GFSH simulations, we implicitly assume that the decoherence rate is the same as the hopping rate, i.e., the elastic and inelastic electron-phonon scattering timescales are identical. However, decoherence and transition times can differ by orders of magnitude. Transitions across large energy gaps, e.g., the fundamental bandgap, can take nanoseconds, while the corresponding coherence time is femtoseconds. 65,66 In contrast, transitions between closely spaced states inside bands are fast, while coherence is maintained for a long time. Such differences are reflected by the decoherence rates in DISH simulations in addition to FSSH and GFSH. Under the CPA, the decoherence rates are typically estimated as puredephasing times using the optical response theory, on the basis of fluctuations of electronic energy levels.³⁸ Decoherence has a strong influence on quantum transitions, leading to many important phenomena, such as the quantum Zeno and anti-Zeno effects. FSSH and GFSH are reported to overestimate quantum transition rates owing to overcoherence. 70,71 DISH can yield more accurate dynamics results, especially for slow transitions across large energy

gaps, and therefore, it has been widely used in modeling carrier trapping, recombination, and related processes. 72-83 To properly account for decoherence in NA-MD simulations, DISH is developed by resorting to decoherence events to simultaneously switch the PES and modify the wave function. When conjugating DISH with the CPA, the Boltzmann factor is naturally introduced into the wave function propagation by scaling the probabilities of collapsing to higher energy states. The probabilities of collapsing to the occupied state and projecting out an unoccupied state are not modified by the Boltzmann factor, because there is no hopping involved. However, if the occupied state is expected to be projected out, the system needs to choose a new PES depending on the wave function populations, and this switch is accepted with a probability of the Boltzmann factor. Such project out-induced hopping mainly occurs when spreading of the wave function over several states is as fast as decoherence. The effect is negligible in weakly coupled systems and is therefore usually ignored, leading to the simplified DISH.

Figure 4 displays the NA-MD simulation results using this simplified DISH. Although decoherence effects are considered, the electron-hole recombination dynamics does not converge and exhibits a non-monotonic dependence on the number of CB states,

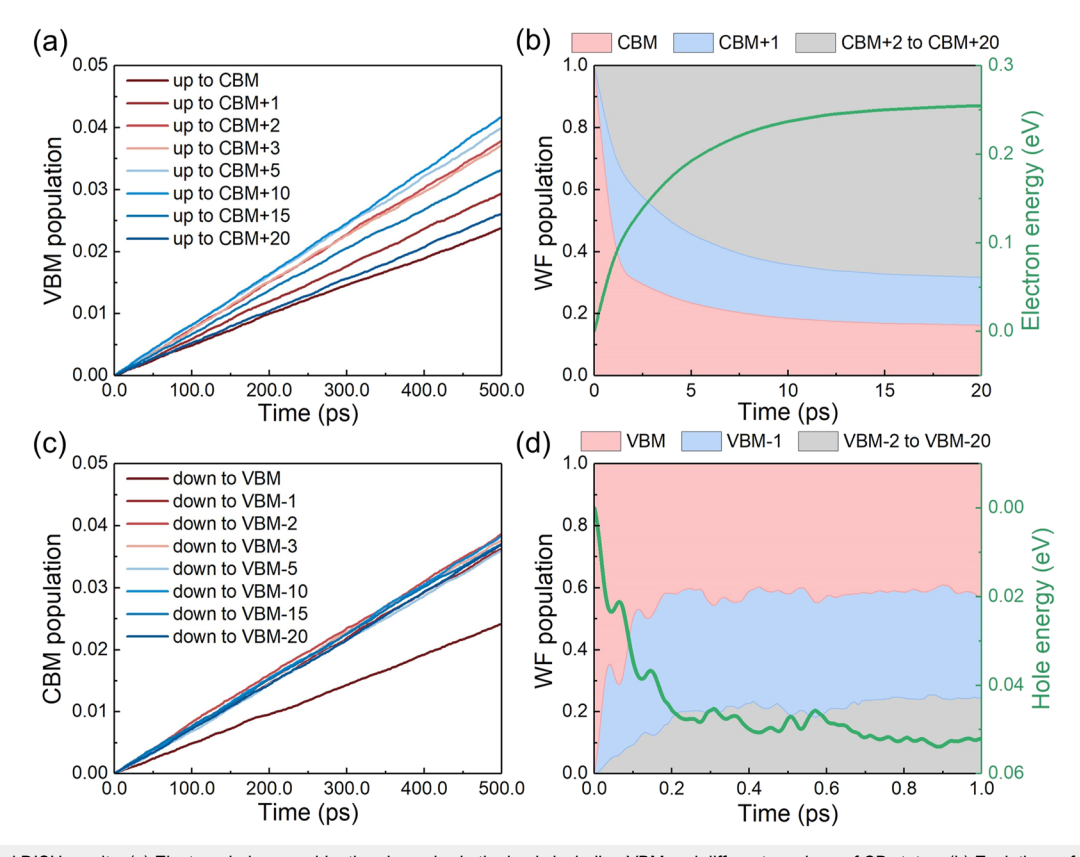


FIG. 4. Simplified DISH results. (a) Electron–hole recombination dynamics in the basis including VBM and different numbers of CB states. (b) Evolutions of state populations and the expectation value of the electron energy with the CB states up to CBM + 20. (c) Electron–hole recombination dynamics in the basis including CBM and different numbers of VB states. (d) Evolutions of state populations and the expectation value of the hole energy with the VB states down to VBM - 20. Similarly to Fig. 2, the recombination dynamics is non-convergent with an increasing number of CB states, and the populations spread unphysically to high energy states, many $k_B T$ away from the band edges. Longer time data are shown in Fig. S7.

as shown in Fig. 4(a). The wave function evolution results plotted in Fig. 4(b) indicate that the wave function leaking issue still exists. The issue remains because project out-induced hops are ignored. Once we include more states above the CBM, the wave function propagates rapidly within the CB, and projecting out events become common. On the one hand, the occupied state, e.g., CBM or CBM $+\,$ 1, is more likely to be projected out due to its reduced population, but the PES is kept there. On the other hand, the higher energy states are also likely to be projected out because the collapse probabilities are significantly reduced by the Boltzmann factor. Therefore, projecting out events are anticipated to be dominant under such circumstances.

Furthermore, the wave function of the system is renormalized after a decohered state is projected out. As a result, the population of the decohered state is transferred to other states. When multiple states above the CBM are included into the simplified DISH simulation, they decohere, and their population is transferred to other states, including the VBM, accelerating the electron–hole recombination. This effect is excluded in the standard DISH simulation, because the wave function population does not leak to high energy states.

The behavior of the electron-hole recombination with an increasing number of VB states is characterized in Figs. 4(c) and

4(d). Similar to FSSH and GFSH, the recombination dynamics converges because the wave function leaking is prevented by the energy gap from VBM - 1 to VBM - 2, Fig. 1(c). Nevertheless, the hole energy deviates from the VBM by much more than $k_{\rm B}T$ at 300 K, indicating that the detailed balance between transitions upward and downward in energy is not properly included. The results of the simplified DISH simulations over 50 ps can be found in Fig. S7.

The project out-induced PES switch is physically valid. For instance, in a two-state system, the project out of one state is equivalent to the collapse to the other state, and the PES should be switched accordingly. Hence, the standard DISH is needed for studying the systems with strong NACs.

The results obtained with the standard DISH are displayed in Fig. 5. The 50 ps simulation data can be found in Fig. S8. The electron–hole recombination dynamics converge with an increasing number of both CB and VB states, and the populations of states far from the band edges remain small. In particular, the inclusion of one more state is sufficient to converge the dynamics in this system because both the VBM and the CBM are doubly degenerate, and the energy gaps to other states are larger than $k_{\rm B}T$; see Fig. 1. Hence, states accessible through thermal excitation are expected to affect the dynamics and need to be included in NA-MD simulations. Note that the recombination becomes several times faster when the

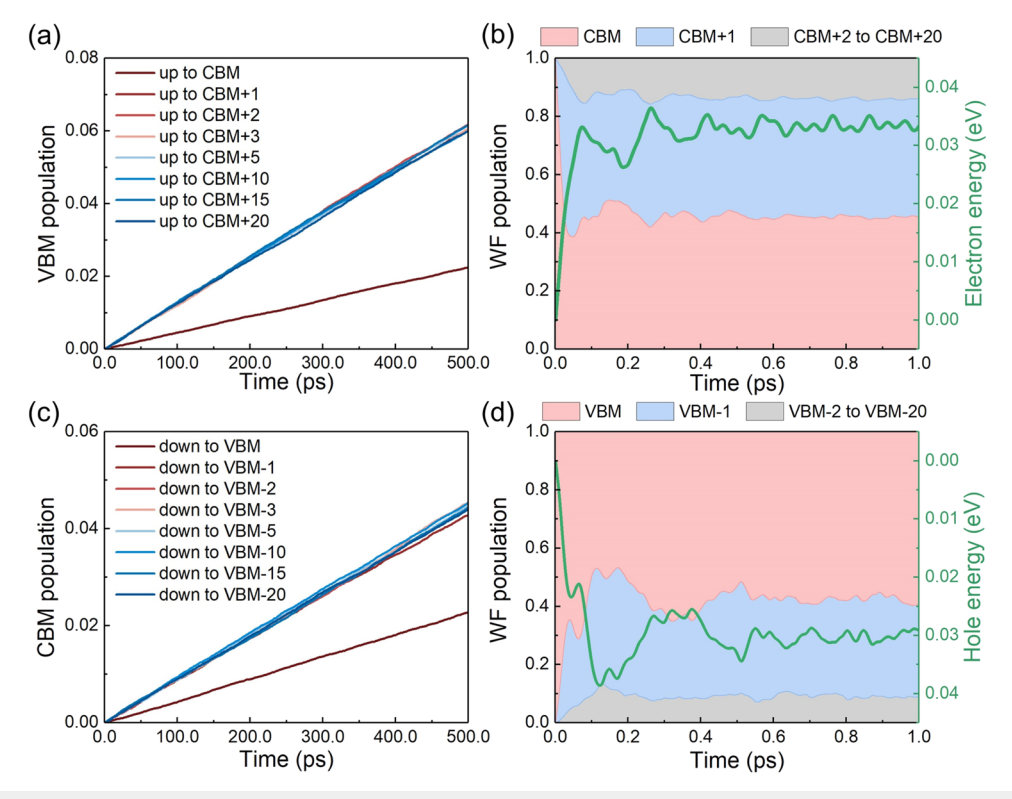


FIG. 5. Standard DISH results. (a) Electron–hole recombination dynamics in the basis including VBM and different numbers of CB states. (b) Evolutions of state populations and the expectation value of the electron energy with the CB states up to CBM + 20. (c) Electron–hole recombination dynamics in the basis including CBM and different numbers of VB states. (d) Evolutions of state populations and the expectation value of the hole energy with the VB states down to VBM – 20. Similarly to Fig. 3, the dynamics converge with an increasing number of CB and VB states, the populations remain close to the band edges, and the energy decays at long times, Fig. S8.

simulation basis is increased beyond just the VBM and CBM, indicating a significant role of intraband wave function propagation in this process. Similar acceleration effects are also observed in the FSSH and GFSH simulations. In the standard DISH, projecting out the occupied state implies that the system is no longer on this PES but remains in a superposition of the other states. Therefore, the system is expected to switch to another PES depending on the wave function population of each state. Changing the PES is restricted by the energy conservation requirement, which is realized by accepting the switch with a probability of the Boltzmann factor under the CPA. If the switch is rejected, the system collapses to the currently occupied state. This action prevents the wave function from leaking to higher energy states and synchronizes it with the PES constantly. Moreover, Figs. 5(b) and 5(d) show that the energies of electron and hole remain within about k_BT from the band edges, indicating that the Boltzmann distribution is satisfied. These results demonstrate that the standard DISH can simulate successfully both fast intraband equilibration and slow interband transitions simultaneously.

It should be pointed out that due to the high density of state in bands, their identification in the adiabatic representation can present a problem. A closely related issue arises in the calculation of NAC, giving rise to the so-called trivial⁸⁴ or unavoided⁸⁵ crossings. In addition, because adiabatic wave functions are defined up to a phase, or sign, in the real-valued case, accurate calculation of NAC requires tracking of adiabatic state phase. To address all these issues, we employ the state tracking algorithm, ^{85,86} which maintains the identity (localization) of individual states. As shown in Fig. S2(b), NACs between the CB states and the VBM are similar. The same is true for NACs between the VB states and CBM. Even if at a given moment in time, the populations of densely spaced states within several $k_B T$ near band edges are not fully accurate, they are distributed according to Boltzmann statistics, and the average rate of transitions across the bandgap is obtained accurately.

FSSH, GFSH, and DISH algorithms within the CPA

Conservation of the quantum-classical energy is achieved in NA-MD by rescaling of the classical velocity after a quantum transition.35 If the transition happens upward in energy, and there is not enough kinetic energy associated with the component of the classical velocity parallel to the NAC to account for the increase in the quantum energy, the hop is rejected. For large systems, the probability to have the kinetic energy needed is Boltzmann, and the system reaches thermodynamic equilibrium in the long-time limit. The detailed balance between quantum transitions upward and downward in energy is achieved under the CPA by scaling the hopping probabilities upward in energy directly with the Boltzmann factor. When hops are also associated with decoherence events, care should be taken in treating simultaneously Boltzmann scaling and decoherence. In particular, when projecting out the occupied state in DISH, the probabilities cannot be scaled by the Boltzmann factor directly, and a more complex procedure is needed.

Generally, for FSSH, GFSH, and DISH, calculation of the SH probability is divided into two steps. First, the expected action is determined by the standard SH probabilities. Second, this action is accepted with a probability of the Boltzmann factor. If the expected action is rejected in the second step, then the opposite action from the first step is accepted. For FSSH and GFSH, the hopping only

occurs when it is accepted in both steps. For DISH, rejecting the expected action changes the decoherence event between projecting onto the decohering state and projecting it out. The flow charts of these algorithms are shown in Figs. 6 and 7, and a description is provided below.

1. Initialize the PES and the wave function of the system. The wave function is expanded into a set of adiabatic states as $\psi(t) = c_1(t)\phi_1 + c_2(t)\phi_2 + c_3(t)\phi_3 + \cdots + c_N(t)\phi_N$, where $c_i(t)$ is the coefficient of the adiabatic state ϕ_i . The wave function can be defined using state vectors as

$$\psi(t) = \begin{bmatrix} c_{1}(t) \\ c_{2}(t) \\ c_{3}(t) \\ \vdots \\ c_{N}(t) \end{bmatrix} = c_{1}(t) \begin{bmatrix} 1 \\ 0 \\ 0 \\ \vdots \\ 0 \end{bmatrix} + c_{2}(t) \begin{bmatrix} 0 \\ 1 \\ 0 \\ \vdots \\ 0 \end{bmatrix} + c_{3}(t) \begin{bmatrix} 0 \\ 0 \\ 1 \\ \vdots \\ 0 \end{bmatrix}$$

$$+ \cdots c_{N}(t) \begin{bmatrix} 0 \\ 0 \\ 0 \\ \vdots \\ 1 \end{bmatrix}, \qquad (12)$$

where each adiabatic state ϕ_i corresponds to a basis vector with the ith non-zero element. We use a set $\{AS\} = \{1, 2, 3, \dots, N\}$ to represent the indexes of these adiabatic states. To initialize

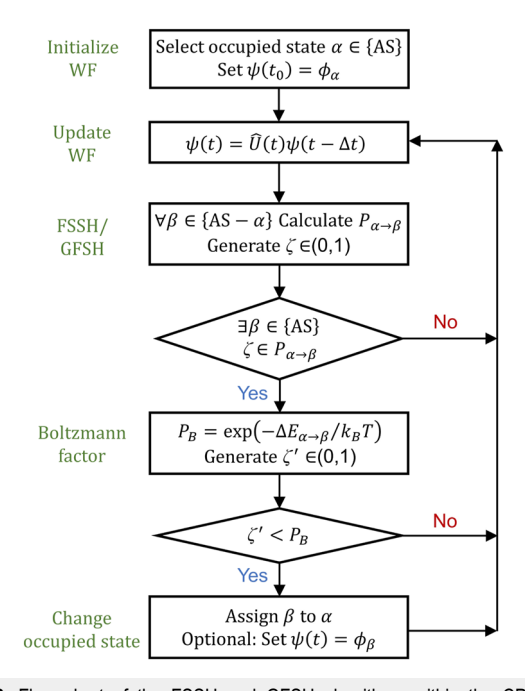


FIG. 6. Flow chart of the FSSH and GFSH algorithms within the CPA. The green color text describes algorithmic steps, and yes/no represents branching that depends on the generated random number.

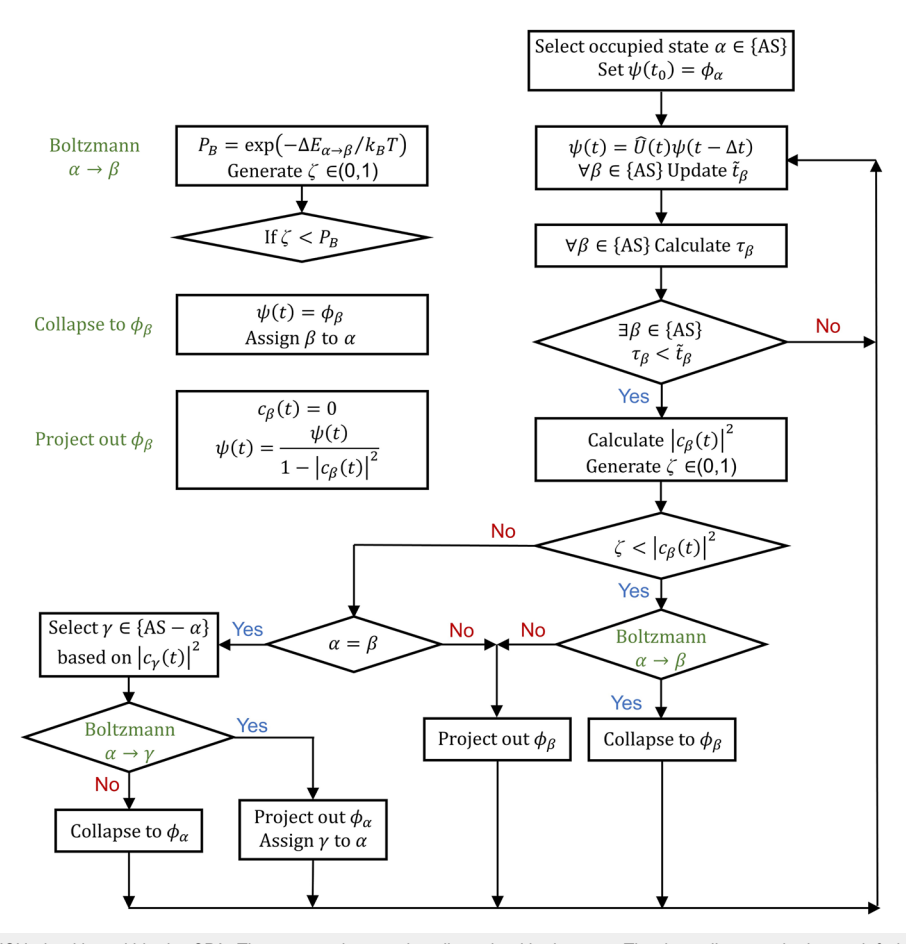


FIG. 7. Flow chart of the DISH algorithm within the CPA. The green color text describes algorithmic steps. The three diagrams in the top left define operations used in the flow chart. Yes/no represents branching that depends on the generated random number.

- the system, state α is selected from {AS} to identify the PES, and the initial wave function $\psi(t_0)$ is set to ϕ_{α} .
- 2. Propagate the wave function according to the TD-SE and update the coefficients of the adiabatic states. In DISH, the time interval of each state from the last decoherence event \tilde{t} is also updated.
- 3. Identify the expected action according to the SH probabilities. In FSSH and GFSH, the hopping probabilities between the occupied state and other states are calculated, and the expected action is determined by a random number between 0 and 1. If this random number falls in the range of probability of hopping to another state, the system is expected to switch to the corresponding PES, otherwise the simulation returns to step 2. In DISH, if \tilde{t} of any state is larger than its decoherence time, the simulation moves forward to specify the decoherence event, otherwise the simulation returns to step 2. The system collapses to the decohering state with the probability of its wave function population, determined by a random number between 0 and 1. If more than one state satisfies this criterion, one of them is selected to undergo decoherence based on this random number and the state populations. If the random
- number does not lead to system collapse to the decohering state, this state is expected to be projected out. Projecting out the occupied state requires switching the PES to one of the other states based on their populations.
- Decide the action according to the Boltzmann factor. The Boltzmann factor is calculated from the energy difference between the initial and final PESs to accept the expected action. Only PES switches with positive energy changes can be rejected because the Boltzmann probabilities are less than 1. In FSSH and GFSH, another random number between 0 and 1 is generated for this decision. If the random number is less than the Boltzmann factor, the hopping is accepted, otherwise, the hopping is rejected and the simulation returns to step 2. In DISH, the wave function collapse is accepted according to the Boltzmann factor as in FSSH and GFSH. Rejecting the collapse leads to projecting out the decohering state. Collapsing the wave function to the occupied state and projecting out an unoccupied state are directly accepted because the PES remains unchanged (i.e., the Boltzmann factor is 1). Projecting out the occupied state is expected to switch the PES and is accepted based on the Boltzmann factor. If

- projecting out the occupied state is rejected, the system collapses to the occupied state.
- 5. Switch the PES and modify the wave function. In FSSH and GFSH, the accepted hopping simply switches the PES to the newly occupied state β . It is optional to collapse the wave function to the new state by setting $\psi(t)$ to ϕ_{β} . Then, the simulation returns to step 2. In DISH, the collapse to state β simultaneously switches the PES to that state and sets the wave function $\psi(t)$ to ϕ_{β} . If the decohering state β is projected out, its coefficient $c_{\beta}(t)$ is set to 0 and the wave function is renormalized. The PES is switched only when β is the currently occupied state. Next, \hat{t} of the decohering state is set to 0, and the simulation returns to step 2.

CONCLUSIONS

In summary, we have demonstrated that the inclusion of decoherence effects is essential for converging NA-MD simulations with an increasing number of states. To satisfy energy conservation in NA-MD, the transition probabilities to higher energy states are reduced to realize the Boltzmann distribution at equilibrium. Hence, the high energy states should not influence the quantum dynamics because of their low populations, and convergence with an increasing number of states should be achieved. However, because the standard TD-SE is unitary and does not include coupling to a bath and, more specifically, the Boltzmann factor is not accounted for in the TD-SE, wave functions can propagate to any state regardless of the energy range. Consequently, the Boltzmann distribution is not achieved, and the results do not converge as the number of states is increased. Decoherence modifies the wave function, making its evolution non-unitary. The wave function collapse caused by decoherence, in combination with the detailed balance between transitions upward and downward in energy during the collapse, suppresses uncontrolled spreading of populations to higher energy states and achieves convergence and thermodynamic equilibrium. Taking the intra- and interband carrier dynamics in MoS2 as an example, we show that standard FSSH, GFSH, and simplified DISH suffer from unrestricted wave function leaking to higher energy states. If decoherence is incorporated into FSSH and GFSH, or DISH is carried out in the full formulation, the correct physical behavior is restored, demonstrating both convergence with the number of states for interband recombination and Boltzmann equilibrium for intraband dynamics. The simultaneous convergence of the fast and slow processes in a typical material indicates that the methods work well and are robust. The CPA employed in our calculations does not influence the unphysical wave function propagation to higher energy states. The wave function leaking arises due to the unitary nature of the TD-SE, regardless of the nature of the atomic trajectory that determines the parametric dependence of the TD-SE on atomic coordinates. Hence, if decoherence and Boltzmann factor (or hop rejection if CPA is not used) are not properly incorporated, and there are many excited states close in energy, the NA-MD simulation convergence problem identified here will be present, regardless of whether the CPA is used or not. The converged interband electron-hole recombination dynamics are several times faster than the two-state simulation results due to additional decay channels, emphasizing the importance of achieving NA-MD

convergence with the number of states. While the simplified DISH can provide reasonable results in simulations involving few states, the standard DISH has to be performed to obtain converged results. DISH also gives accurate and converged results for other processes besides electron–hole recombination, including hot electron relaxation, charge trapping, charge transfer, and Auger-type processes. The reported work highlights the crucial role of decoherence in NA-MD simulations and provides rigorous means for modeling complex quantum processes in condensed phase and nanoscale systems.

SUPPLEMENTARY MATERIAL

The supplementary material contains a comparison of results with original and ten times enlarged non-adiabatic coupling, evolution of energy levels over 5 ps, and additional NA-MD simulation results.

ACKNOWLEDGMENTS

This research was supported in part through computational resources of HPC facilities at HSE University. A.S.V. acknowledges the support from the Basic Research Program of HSE University. O.V.P. acknowledges the support of the US National Science Foundation, Grant No. CHE-2154367.

AUTHOR DECLARATIONS

Conflict of Interest

The authors have no conflicts to disclose.

Author Contributions

Dongyu Liu: Conceptualization (equal); Software (equal); Writing – original draft (equal). **Bipeng Wang**: Software (equal). **Andrey S. Vasenko**: Conceptualization (equal); Writing – review & editing (equal). **Oleg V. Prezhdo**: Conceptualization (equal); Writing – review & editing (equal).

DATA AVAILABILITY

The data that support the findings of this study are available from the corresponding authors upon reasonable request.

REFERENCES

- ¹T. R. Nelson, A. J. White, J. A. Bjorgaard, A. E. Sifain, Y. Zhang, B. Nebgen, S. Fernandez-Alberti, D. Mozyrsky, A. E. Roitberg, and S. Tretiak, "Nonadiabatic excited-state molecular dynamics: Theory and applications for modeling photophysics in extended molecular materials," Chem. Rev. 120, 2215–2287 (2020).
- ²S. Giannini and J. Blumberger, "Charge transport in organic semiconductors: The perspective from nonadiabatic molecular dynamics," Acc. Chem. Res. 55, 819–830 (2022).
- ³L. Wang, R. Long, and O. V. Prezhdo, "Time-domain *ab initio* modeling of photoinduced dynamics at nanoscale interfaces," Annu. Rev. Phys. Chem. **66**, 549–579 (2015)

- ⁴ A. W. Jasper, S. Nangia, C. Y. Zhu, and D. G. Truhlar, "Non-Born-Oppenheimer molecular dynamics," ChemInform 37, 101–108 (2006).
- ⁵M. Barbatti, "Nonadiabatic dynamics with trajectory surface hopping method," WIRES Comput. Mol. Sci. 1, 620–633 (2011).
- ⁶S. Mai, P. Marquetand, and L. González, "Nonadiabatic dynamics: The SHARC approach," WIREs Comput. Mol. Sci. **8**, e1370 (2018).
- ⁷O. V. Prezhdo, "Modeling non-adiabatic dynamics in nanoscale and condensed matter systems," Acc. Chem. Res. **54**, 4239–4249 (2021).
- ⁸J. C. Tully, "Mixed quantum-classical dynamics," Faraday Discuss. **110**, 407–419 (1998).
- ⁹R. Kapral and G. Ciccotti, "Mixed quantum-classical dynamics," J. Chem. Phys. 110, 8919–8929 (1999).
- ¹⁰J. C. Tully, "Perspective: Nonadiabatic dynamics theory," J. Chem. Phys. 137, 22A301 (2012).
- ¹¹R. Crespo-Otero and M. Barbatti, "Recent advances and perspectives on nonadiabatic mixed quantum-classical dynamics," Chem. Rev. 118, 7026–7068 (2018).
- ¹²S. Mai and L. González, "Molecular photochemistry: Recent developments in theory," Angew. Chem., Int. Ed. **59**, 16832–16846 (2020).
- ¹³W. R. Duncan and O. V. Prezhdo, "Theoretical studies of photoinduced electron transfer in dye-sensitized TiO₂," Annu. Rev. Phys. Chem. **58**, 143–184 (2007).
- ¹⁴R. Long, O. V. Prezhdo, and W. Fang, "Nonadiabatic charge dynamics in novel solar cell materials," WIREs Comput. Mol. Sci. 7, e1305 (2017).
- ¹⁵W. Li, Y. She, A. S. Vasenko, and O. V. Prezhdo, "*Ab initio* nonadiabatic molecular dynamics of charge carriers in metal halide perovskites," Nanoscale 13, 10239–10265 (2021).
- ¹⁶J. Behler, "Perspective: Machine learning potentials for atomistic simulations," J. Chem. Phys. 145, 170901 (2016).
- ¹⁷J. Westermayr, M. Gastegger, K. T. Schütt, and R. J. Maurer, "Perspective on integrating machine learning into computational chemistry and materials science," J. Chem. Phys. **154**, 230903 (2021).
- ¹⁸B. Bauer, S. Bravyi, M. Motta, and G. K.-L. Chan, "Quantum algorithms for quantum chemistry and quantum materials science," Chem. Rev. **120**, 12685–12717 (2020).
- ¹⁹W. Mi, K. Luo, S. B. Trickey, and M. Pavanello, "Orbital-free density functional theory: An attractive electronic structure method for large-scale first-principles simulations," Chem. Rev. **123**, 12039–12104 (2023).
- ²⁰ H. Li, Z. Wang, N. Zou, M. Ye, R. Xu, X. Gong, W. Duan, and Y. Xu, "Deep-learning density functional theory Hamiltonian for efficient *ab initio* electronic-structure calculation," Nat. Comput. Sci. **2**, 367–377 (2022).
- ²¹ X. Gong, H. Li, N. Zou, R. Xu, W. Duan, and Y. Xu, "General framework for E(3)-equivariant neural network representation of density functional theory Hamiltonian," Nat. Commun. 14, 2848 (2023).
- ²²L. Zhang, J. Han, H. Wang, R. Car, and W. E, "Deep potential molecular dynamics: A scalable model with the accuracy of quantum mechanics," Phys. Rev. Lett. 120, 143001 (2018).
- ²³T. Mueller, A. Hernandez, and C. Wang, "Machine learning for interatomic potential models," J. Chem. Phys. **152**, 050902 (2020).
- ²⁴O. T. Unke, S. Chmiela, H. E. Sauceda, M. Gastegger, I. Poltavsky, K. T. Schütt, A. Tkatchenko, and K.-R. Müller, "Machine learning force fields," Chem. Rev. 121, 10142–10186 (2021).
- ²⁵ F. P. García de Arquer, D. V. Talapin, V. I. Klimov, Y. Arakawa, M. Bayer, and E. H. Sargent, "Semiconductor quantum dots: Technological progress and future challenges," Science 373, eaaz8541 (2021).
- ²⁶O. V. Prezhdo, "Photoinduced dynamics in semiconductor quantum dots: Insights from time-domain *ab initio* studies," Acc. Chem. Res. **42**, 2005–2016 (2009).
- ²⁷K. Hyeon-Deuk, J. Kim, and O. V. Prezhdo, "Ab initio analysis of auger-assisted electron transfer," J. Phys. Chem. Lett. 6, 244–249 (2015).
- ²⁸ J. R. Schaibley, H. Yu, G. Clark, P. Rivera, J. S. Ross, K. L. Seyler, W. Yao, and X. Xu, "Valleytronics in 2D materials," Nat. Rev. Mater. 1, 16055 (2016).
- ²⁹Z. Zheng, Y. Shi, J.-J. Zhou, O. V. Prezhdo, Q. Zheng, and J. Zhao, "Ab initio real-time quantum dynamics of charge carriers in momentum space," Nat. Comput. Sci. 3, 532–541 (2023).

- ³⁰D. Huang, J. Choi, C.-K. Shih, and X. Li, "Excitons in semiconductor Moiré superlattices," Nat. Nanotechnol. 17, 227–238 (2022).
- ³¹H. Guo, X. Zhang, and G. Lu, "Shedding light on Moiré excitons: A first-principles perspective," Sci. Adv. 6, eabc5638 (2020).
- ³²D. Lembke, S. Bertolazzi, and A. Kis, "Single-layer MoS₂ electronics," Acc. Chem. Res. **48**, 100–110 (2015).
- 33 H. Wang, C. Li, P. Fang, Z. Zhang, and J. Z. Zhang, "Synthesis, properties, and optoelectronic applications of two-dimensional MoS₂ and MoS₂-based heterostructures," Chem. Soc. Rev. 47, 6101–6127 (2018).
- ³⁴J. Kwon, M. Seol, J. Yoo, H. Ryu, D.-S. Ko, M.-H. Lee, E. K. Lee, M. S. Yoo, G.-H. Lee, H.-J. Shin, J. Kim, and K.-E. Byun, "200-mm-wafer-scale integration of polycrystalline molybdenum disulfide transistors," Nat. Electron. 7, 356–364 (2024).
- ³⁵J. C. Tully, "Molecular dynamics with electronic transitions," J. Chem. Phys. 93, 1061–1071 (1990).
- ³⁶L. Wang, D. Trivedi, and O. V. Prezhdo, "Global flux surface hopping approach for mixed quantum-classical dynamics," J. Chem. Theory Comput. 10, 3598–3605 (2014).
- ³⁷H. M. Jaeger, S. Fischer, and O. V. Prezhdo, "Decoherence-induced surface hopping," J. Chem. Phys. **137**, 22A545 (2012).
- ³⁸ A. V. Akimov and O. V. Prezhdo, "The PYXAID program for non-adiabatic molecular dynamics in condensed matter systems," J. Chem. Theory Comput. 9, 4959–4972 (2013).
- ³⁹A. V. Akimov and O. V. Prezhdo, "Advanced capabilities of the PYXAID program: Integration schemes, decoherence effects, multiexcitonic states, and field-matter interaction," J. Chem. Theory Comput. 10, 789–804 (2014).
- ⁴⁰Q. Zheng, W. Chu, C. Zhao, L. Zhang, H. Guo, Y. Wang, X. Jiang, and J. Zhao, "Ab initio nonadiabatic molecular dynamics investigations on the excited carriers in condensed matter systems," WIRES Comput. Mol. Sci. 9, e1411 (2019).
- ⁴¹ A. V. Akimov and O. V. Prezhdo, in *Encyclopedia of Nanotechnology*, edited by B. Bhushan (Springer Netherlands, Dordrecht, 2016), pp. 1–20.
- ⁴²B. Smith and A. V. Akimov, "Modeling nonadiabatic dynamics in condensed matter materials: Some recent advances and applications," J. Phys.: Condens. Matter 32, 073001 (2020).
- ⁴³D. J. Trivedi, L. J. Wang, and O. V. Prezhdo, "Auger-mediated electron relaxation is robust to deep hole traps: Time-domain *ab initio* study of CdSe quantum dots," Nano Lett. 15, 2086–2091 (2015).
- ⁴⁴J. E. Subotnik, A. Jain, B. Landry, A. Petit, W. Ouyang, and N. Bellonzi, "Understanding the surface hopping view of electronic transitions and decoherence," Annu. Rev. Phys. Chem. **67**, 387–417 (2016).
- ⁴⁵T. Nelson, S. Fernandez-Alberti, A. E. Roitberg, and S. Tretiak, "Nonadiabatic excited-state molecular dynamics: Treatment of electronic decoherence," J. Chem. Phys. 138, 224111 (2013).
- ⁴⁶G. C. Ghirardi, P. Pearle, and A. Rimini, "Markov processes in Hilbert space and continuous spontaneous localization of systems of identical particles," Phys. Rev. A 42, 78–89 (1990).
- ⁴⁷M. B. Plenio and P. L. Knight, "The quantum-jump approach to dissipative dynamics in quantum optics," Rev. Mod. Phys. **70**, 101–144 (1998).
- ⁴⁸O. V. Prezhdo, "Mean field approximation for the stochastic Schrodinger equation," J. Chem. Phys. 111, 8366–8377 (1999).
- ⁴⁹M. Moodley and F. Petruccione, "Stochastic wave-function unraveling of the generalized Lindblad master equation," Phys. Rev. A **79**, 042103 (2009).
- 50 S. Gumber and O. V. Prezhdo, "Zeno and anti-zeno effects in nonadiabatic molecular dynamics," J. Phys. Chem. Lett. 14, 7274–7282 (2023).
- ⁵¹ S. Pal, P. Nijjar, T. Frauenheim, and O. V. Prezhdo, "Atomistic analysis of room temperature quantum coherence in two-dimensional CdSe nanostructures," Nano Lett. 17, 2389–2396 (2017).
- ⁵²G. Kresse and J. Hafner, "Ab initio molecular dynamics for liquid metals," Phys. Rev. B 47, 558–561 (1993).
- ⁵³G. Kresse and J. Hafner, "Ab initio molecular-dynamics simulation of the liquid-metal–amorphous-semiconductor transition in germanium," Phys. Rev. B 49, 14251–14269 (1994).
- ⁵⁴G. Kresse and J. Furthmüller, "Efficient iterative schemes for *ab initio* total-energy calculations using a plane-wave basis set," Phys. Rev. B **54**, 11169–11186 (1996).

- 55 G. Kresse and J. Furthmüller, "Efficiency of ab-initio total energy calculations for metals and semiconductors using a plane-wave basis set," Comput. Mater. Sci.
- ⁵⁶P. E. Blöchl, "Projector augmented-wave method," Phys. Rev. B 50, 17953-17979 (1994).
- $^{\bf 57}{\rm G.}$ Kresse and D. Joubert, "From ultrasoft pseudopotentials to the projector augmented-wave method," Phys. Rev. B 59, 1758-1775 (1999).
- 58 W. B. Chu, Q. J. Zheng, A. V. Akimov, J. Zhao, W. A. Saidi, and O. V. Prezhdo, "Accurate computation of nonadiabatic coupling with projector augmented-wave pseudopotentials," J. Phys. Chem. Lett. 11, 10073-10080 (2020).
- ⁵⁹ W. B. Chu and O. V. Prezhdo, "Concentric approximation for fast and accurate numerical evaluation of nonadiabatic coupling with projector augmented-wave pseudopotentials," J. Phys. Chem. Lett. 12, 3082–3089 (2021).

 60 J. P. Perdew, K. Burke, and M. Ernzerhof, "Generalized gradient approximation
- made simple," Phys. Rev. Lett. 77, 3865-3868 (1996).
- ⁶¹T. Ozaki, "Variationally optimized atomic orbitals for large-scale electronic structures," Phys. Rev. B 67, 155108 (2003).
- ⁶²T. Ozaki and H. Kino, "Numerical atomic basis orbitals from H to Kr," Phys. Rev. B 69, 195113 (2004).
- ⁶³I. Morrison, D. M. Bylander, and L. Kleinman, "Nonlocal Hermitian normconserving Vanderbilt pseudopotential," Phys. Rev. B 47, 6728-6731 (1993).
- ⁶⁴M. Shakiba, E. Stippell, W. Li, and A. V. Akimov, "Nonadiabatic molecular dynamics with extended density functional tight-binding: Application to nanocrystals and periodic solids," J. Chem. Theory Comput. 18, 5157-5180
- ⁶⁵L. Q. Li, R. Long, and O. V. Prezhdo, "Why chemical vapor deposition grown MoS₂ samples outperform physical vapor deposition samples: Time-domain ab initio analysis," Nano Lett. 18, 4008-4014 (2018).
- ⁶⁶Y. L. Liu, R. Long, W. H. Fang, and O. V. Prezhdo, "Nuclear quantum effects prolong charge carrier lifetimes in hybrid organic-inorganic perovskites," J. Am. Chem. Soc. **145**, 14112–14123 (2023).
- ⁶⁷M. P. A. Branderhorst, P. Londero, P. Wasylczyk, C. Brif, R. L. Kosut, H. Rabitz, and I. A. Walmsley, "Coherent control of decoherence," Science 320, 638-643
- ⁶⁸ A. Chenu and G. D. Scholes, "Coherence in energy transfer and photosynthesis," Annu. Rev. Phys. Chem. 66, 69-96 (2015).
- ⁶⁹S. V. Kilina, A. J. Neukirch, B. F. Habenicht, D. S. Kilin, and O. V. Prezhdo, "Quantum zeno effect rationalizes the phonon bottleneck in semiconductor quantum dots," Phys. Rev. Lett. 110, 180404 (2013).
- ⁷⁰B. J. Schwartz, E. R. Bittner, O. V. Prezhdo, and P. J. Rossky, "Quantum decoherence and the isotope effect in condensed phase nonadiabatic molecular dynamics simulations," J. Chem. Phys. 104, 5942-5955 (1996).
- ⁷¹O. V. Prezhdo and P. J. Rossky, "Evaluation of quantum transition rates from quantum-classical molecular dynamics simulations," J. Chem. Phys. 107, 5863-5878 (1997).

- 72 K. Hyeon-Deuk and O. V. Prezhdo, "Time-domain ab initio study of auger and phonon-assisted auger processes in a semiconductor quantum Dot," Nano Lett. 11, 1845-1850 (2011).
- ⁷³Z. S. Zhang, L. H. Liu, W. H. Fang, R. Long, M. V. Tokina, and O. V. Prezhdo, "Plasmon-mediated electron injection from Au nanorods into MoS₂: Traditional versus photoexcitation mechanism," Chem 4, 1112-1127 (2018).
- 74R. Shi, A. S. Vasenko, R. Long, and O. V. Prezhdo, "Edge influence on charge carrier localization and lifetime in CH3NH3PbBr3 perovskite: Ab initio quantum dynamics simulation," J. Phys. Chem. Lett. 11, 9100-9109 (2020).
- ⁷⁵Y. Wu, W. Chu, A. S. Vasenko, and O. V. Prezhdo, "Common defects accelerate charge carrier recombination in CsSnI₃ without creating mid-gap states," J. Phys. Chem. Lett. 12, 8699-8705 (2021).
- ⁷⁶C. Cheng, W. H. Fang, R. Long, and O. V. Prezhdo, "Water splitting with a single-atom Cu/TiO2 photocatalyst: Atomistic origin of high efficiency and proposed enhancement by spin selection," Jacs Au 1, 550–559 (2021). ⁷⁷S. Agrawal, A. S. Vasenko, D. J. Trivedi, and O. V. Prezhdo, "Charge carrier
- nonadiabatic dynamics in non-metal doped graphitic carbon nitride," J. Chem. Phys. 156, 094702 (2022).
- ⁷⁸R. Shi, W.-H. Fang, A. S. Vasenko, R. Long, and O. V. Prezhdo, "Efficient passivation of DY center in CH3NH3PbBr3 by chlorine: Quantum molecular dynamics," Nano Res. 15, 2112-2122 (2022).
- 79 X. Zhao, A. S. Vasenko, O. V. Prezhdo, and R. Long, "Anion doping delays nonradiative electron-hole recombination in Cs-based all-inorganic perovskites: Time domain ab initio analysis," J. Phys. Chem. Lett. 13, 11375-11382 (2022).
- 80 R. Shi, Q. Fang, A. S. Vasenko, R. Long, W.-H. Fang, and O. V. Prezhdo, "Structural disorder in higher-temperature phases increases charge carrier lifetimes in metal halide perovskites," J. Am. Chem. Soc. 144, 19137-19149
- ⁸¹D. Liu, C. M. Perez, A. S. Vasenko, and O. V. Prezhdo, "Ag-Bi charge redistribution creates deep traps in defective Cs2AgBiBr6: Machine learning analysis of density functional theory," J. Phys. Chem. Lett. 13, 3645-3651 (2022).
- 82 B. Wang, Y. Wu, D. Liu, A. S. Vasenko, D. Casanova, and O. V. Prezhdo, "Efficient modeling of quantum dynamics of charge carriers in materials using short nonequilibrium molecular dynamics," J. Phys. Chem. Lett. 14, 8289-8295
- 83 W. Li, T. Xue, C. Mora-Perez, and O. V. Prezhdo, "Ab initio quantum dynamics of plasmonic charge carriers," Trends Chem. 5, 634-645 (2023).
- ⁸⁴L. Wang and O. V. Prezhdo, "A Simple solution to the trivial crossing problem in surface hopping," J. Phys. Chem. Lett. 5, 713-719 (2014).
- 85 S. Fernandez-Alberti, A. E. Roitberg, T. Nelson, and S. Tretiak, "Identification of unavoided crossings in nonadiabatic photoexcited dynamics involving multiple electronic states in polyatomic conjugated molecules," J. Chem. Phys. 137, 014512
- ⁸⁶A. V. Akimov, "A simple phase correction makes a big difference in nonadiabatic molecular dynamics," J. Phys. Chem. Lett. 9, 6096-6102 (2018).